Int. J. Heat Mass Transfer. Vol. 28, No. 9, pp. 1699–1709, 1985
Printed in Great Britain

0017-9310/85 $3.00 + 0.00

Analysis of laminar mixed convection in shrouded arrays of heated rectangular blocks

MARK E. BRAATEN and SUHAS V. PATANKAR
Department of Mechanical Engineering, University of Minnesota, Minneapolis, MN 55455, U.S.A.

(*Received* 20 *September* 1984 *and in final form* 20 *February* 1985)

Abstract—The effect of buoyancy on the flow and heat transfer in shrouded arrays of rectangular blocks is studied numerically. The problem considered is relevant to the cooling of electronic equipment made up of components mounted on horizontal circuit boards. The effects of orientation of the blocks, heat conduction within the shrouds, and fluid properties are considered. Detailed velocity and temperature fields are computed. The results show that buoyancy leads to a significant enhancement in heat transfer along with a smaller increase in pressure drop, with the greatest enhancement found when the heated blocks face upward. The secondary flow forms single-eddy patterns at low Rayleigh numbers, and both single- and multiple-eddy patterns at higher Rayleigh numbers.

INTRODUCTION

RECENT advances in semiconductor technology have led to increasing miniaturization in circuit design. As electronic components are made smaller, the amount of heat that must be dissipated per unit volume of a device increases dramatically. For example, the peak heat fluxes in a recent computer circuit are 10 times greater than those in an older computer [1]. Forced convection cooling of the circuitry is commonly used to maintain the desired operating temperature in such a device. With increased heat fluxes within the device, the buoyancy effects in the cooling fluid assume greater importance, leading to a mixed convection situation. The purpose in the present work is to examine the effects of buoyancy on the flow and heat transfer in a geometry representative of that existing in modern electronic equipment.

Many modern electronic devices are made up of heat producing components mounted on closely-spaced circuit boards, as typified by the computer circuit shown in Fig. 1. The electronic components act as local heat sources, so that the heat flux dissipated into the cooling fluid is highly nonuniform. The principal effect of buoyancy on the flow in such a device is the establishment of a secondary flow in the passage cross-section.

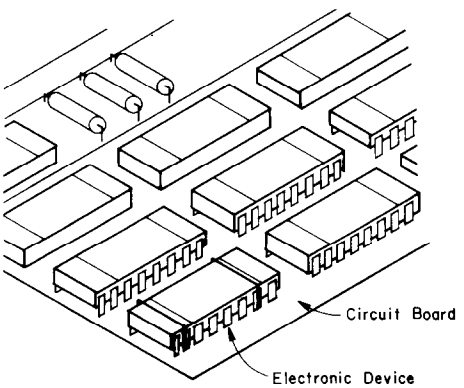

FIG. 1. Typical computer circuit.

A two-dimensional idealization of this situation is shown schematically in Fig. 2(a). It consists of repeated layers of parallel plate shrouds, with large rectangular blocks mounted on the shrouds, spaced periodically in the spanwise direction. This geometry can be considered as a special case of that shown in Fig. 1, in which the components are all the same size and in which streamwise spacing between adjacent components is very small relative to their length. The analysis in the present paper pertains to this geometry; the primary flow is considered to be in the direction normal to the plane of the figure. The analysis of the flow in such a geometry also has other applications. Some examples are the flow in a parallel plate channel in which strip heaters have been attached to one plate, or in which one plate is grooved, and the flow in a shrouded array of thick fins.

Laminar *forced* convection in a geometry of this type was studied numerically in [2]. Mixed convection in horizontal flows has been studied by various investigators for the cases of smooth parallel plates and smooth rectangular channels in [3, 4]. The case of mixed convection between parallel plates with local heat sources on the bottom plate was reported in [5].

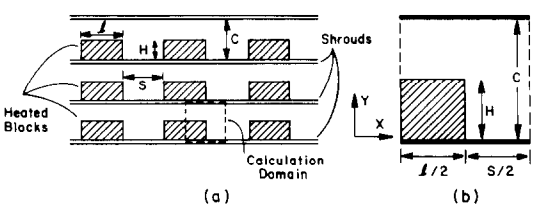

FIG. 2. (a) Geometry under consideration; (b) calculation domain.

NOMENCLATURE

A	cross-sectional area of computational module open to flow, $[c(l+s)-Hl]/2$
A_b	surface area of the block per unit axial length of computational module, $H+l/2$
c	spacing between shrouds
C	dimensionless geometric parameter, c/H
c_p	specific heat at constant pressure
D_h	hydraulic diameter, equation (18)
f	friction factor, equation (17)
g	acceleration due to gravity
h	average heat transfer coefficient, equation (16)
H	height of block
k	thermal conductivity of the fluid
l	horizontal length of heated block
L	dimensionless geometric parameter, l/H
Nu	average Nusselt number, hH/k
Nu_0	average Nusselt number for forced convection
p	pressure
$\bar{p}$	mean pressure averaged over the passage cross-section
p^*	effective pressure, $p+\rho gy$
P	dimensionless pressure, equation (6)
Pr	fluid Prandtl number, ν/α
Q'	heat input per unit axial length of computational module
Ra	Rayleigh number, equation (8)
Re	Reynolds number, $\bar{w}D_h/\nu$
s	spacing between blocks
S	dimensionless geometric parameter, s/H
T	temperature
T_b	bulk fluid temperature
T_w	wall temperature
u, v, w	velocity components in the x, y, z coordinate directions
U, V, W	dimensionless velocities, equations (6) and (7)
x	horizontal coordinate
X	dimensionless horizontal coordinate, x/H
y	vertical coordinate
Y	dimensionless vertical coordinate, y/H
z	axial coordinate
Z	dimensionless axial coordinate, z/H.

Greek symbols

α	thermal diffusivity of the fluid
β	thermal expansion coefficient of the fluid
ν	kinematic viscosity of the fluid
ρ	fluid density
ϕ	dimensionless temperature, equation (7)
ψ	dimensionless stream function, equations (14) and (15)
ψ_m	maximum value of ψ.

Mixed convection in a shrouded array of thin fins was investigated in [6]. Buoyancy effects were found to lead to a significant increase in heat transfer and flow friction over the forced convection values.

The analysis presented here is carried out for laminar flow assuming both hydrodynamically and thermally fully-developed conditions. The rectangular blocks are assumed to contain distributed heat sources of equal strength per unit axial length. The surfaces of the blocks are assumed to be highly conductive relative to the fluid so that the surface temperature of each block is uniform in a given cross-section. The thermal boundary condition is thus one of uniform heat flux per unit axial length, which admits a thermally fully-developed regime even when buoyancy forces are taken into account.

Although the main purpose of these assumptions is to simplify the analysis, they are not unduly unrealistic, and the fundamental nature of the buoyancy effects can still be studied. Consider a circuit such as that depicted in Fig. 1, consisting of long modules lined up end-to-end in regularly spaced rows, with the flow aligned with the main axis of the elements. If the components are metal-cased, their surfaces will be highly conductive so that the surface temperature of each module will be roughly uniform. If the streamwise gaps between the components are small, the three-dimensional effects of streamwise vortices in the gap regions will be small. If the rows of elements are long, fully-developed conditions will then prevail over much of the length of the device. Even for the more general three-dimensional case, the present two-dimensional analysis is expected to provide qualitative guidance about the effects of buoyancy.

Many factors are expected to have a significant effect on the results of this problem. These include the strength of the heating (as characterized by the Rayleigh number), the various geometric parameters that define the passage geometry, the orientation of the rectangular blocks (whether they are mounted facing upward or downward), the conductivity of the shroud material, and the properties of the cooling fluid. Since the effect of the geometric parameters was studied exhaustively for the forced convection case in ref. [2], the focus of this work is on the other factors.

ANALYSIS

Due to the geometrical symmetry of this problem, it is possible to confine the analysis to a typical repeating

module, as shown in Fig. 2(b). As regards the thermal boundary conditions on the shrouds, the two limiting cases of perfectly conducting shrouds and nonconducting shrouds are considered. When the shrouds are perfectly conducting, they attain the same temperature as the surfaces of the blocks (assuming zero contact resistance between the block surface and the shroud). Nonconducting shrouds will have zero heat flux across them. The results for shrouds of finite conductivity are expected to lie between the results presented here for the two limiting cases.

The governing equations for conservation of mass, momentum, and energy are formulated for fully-developed laminar flow. All fluid properties are treated as constant, except the fluid density in the buoyancy term, in accordance with Boussinesq's approximation. The buoyancy term ρg takes the form:

$$\rho g = \rho_w[1-\beta(T-T_w)]g \quad (1)$$

$$= \rho_w g - \rho_w \beta g(T-T_w). \quad (2)$$

The term $\rho_w g$ is absorbed into the pressure term by defining an effective pressure $p^* = p+\rho_w g y$. In accordance with the constant density approximation, the subscript 'w' will subsequently be dropped.

For fully-developed flow all velocity gradients in the axial direction vanish ($\partial u/\partial z = \partial v/\partial z = \partial w/\partial z = 0$). The axial pressure gradient $\partial p/\partial z$ is replaced by $\mathrm{d}\bar{p}/\mathrm{d}z$ (where $\bar{p}$ is the mean pressure averaged over the cross-section of the passage), and is assumed constant. For the given thermal boundary condition of uniform heat flux per unit axial length, all temperatures rise linearly with axial distance, thus:

$$\partial T/\partial z = \mathrm{d}T_w/\mathrm{d}z = \mathrm{d}T_b/\mathrm{d}z. \quad (3)$$

The rate of rise of bulk temperature, found from an overall energy balance, is given by:

$$\mathrm{d}T_b/\mathrm{d}z = Q'/(\rho c_p \bar{w} A). \quad (4)$$

To express the governing equations in dimensionless form, the following quantities are defined:

$$X = x/H \quad Y = y/H \quad S = s/H \quad L = l/H \quad C = c/H \quad (5)$$

$$U = uH/\alpha \quad V = vH/\alpha \quad P = p^*H^2/(\rho\alpha^2) \quad (6)$$

$$\phi = k(T-T_w)/Q' \quad W = \rho v w/(-\mathrm{d}\bar{p}/\mathrm{d}z)/H^2 \quad (7)$$

$$Pr = \nu/\alpha \quad Ra = g\beta Q' H^3/(\alpha\nu k). \quad (8)$$

The substitution of these dimensionless variables into the conservation equations leads to:

$$\frac{\partial U}{\partial X} + \frac{\partial V}{\partial Y} = 0 \quad (9)$$

$$\frac{1}{Pr}\left(U\frac{\partial U}{\partial X} + V\frac{\partial U}{\partial Y}\right) = \frac{1}{Pr}\left(\frac{-\partial P}{\partial X}\right) + \frac{\partial^2 U}{\partial X^2} + \frac{\partial^2 U}{\partial Y^2} \quad (10)$$

$$\frac{1}{Pr}\left(U\frac{\partial V}{\partial X} + V\frac{\partial V}{\partial Y}\right) = \frac{1}{Pr}\left(\frac{-\partial P}{\partial Y}\right) + \frac{\partial^2 V}{\partial X^2} + \frac{\partial^2 V}{\partial Y^2} + Ra\phi \quad (11)$$

$$\frac{1}{Pr}\left(U\frac{\partial W}{\partial X} + V\frac{\partial W}{\partial Y}\right) = 1 + \frac{\partial^2 W}{\partial X^2} + \frac{\partial^2 W}{\partial Y^2} \quad (12)$$

$$U\frac{\partial \phi}{\partial X} + V\frac{\partial \phi}{\partial Y} = \frac{\partial^2 \phi}{\partial X^2} + \frac{\partial^2 \phi}{\partial Y^2} - \left(\frac{H^2}{A}\right)\frac{W}{\bar{W}} \quad (13)$$

where A is the cross-sectional area of the computational module open to flow. The coefficient H^2/A is a function only of the geometric parameters S, L, and C. Thus, the dimensionless equations contain five independent parameters: the geometric parameters S, L and C; the Rayleigh number, and the Prandtl number. In this analysis, the geometric parameters are held fixed, at the following values: $S = 2$, $L = 2$, $C = 2$. This corresponds to a situation where the blocks occupy a large fraction of the cross-sectional area of the flow passage, so that the resulting velocity and temperature fields are severely distorted from those of a parallel plate geometry. Fixing the geometry leaves the Rayleigh and Prandtl numbers as the only parameters of interest. It should be noted from investigation of the above equations that for a given geometry, when the Prandtl number becomes large the terms containing $1/Pr$ vanish, leaving the Rayleigh number as the only independent parameter. It has been found [7] that the Rayleigh number accounts for the major effect of Prandtl number dependence even at rather low Prandtl numbers. It was for this reason that the Rayleigh number was chosen to characterize the strength of the buoyancy effect, rather than the Grashof number used in [6]. It should also be noted, that since the flow is fully developed, the solution is not affected by the Reynolds number of the axial flow. This is a characteristic of all fully-developed duct flows.

For computational convenience, the boundary conditions for the problem are imposed on the nominally rectangular boundary of the domain, shown in Fig. 2(b). The shaded area occupied by the solid is assigned virtually infinite values of viscosity and thermal conductivity. This causes the calculated velocity in the solid to be zero and allows the desired surface temperature to be specified on the nominal boundary. This procedure for embedding solid regions within a flow field has been explained in [8, 9]. The normal velocity u and the normal gradients $\partial v/\partial x$, $\partial w/\partial x$, and $\partial T/\partial x$ are set equal to zero on the symmetry lines. For perfectly conducting shrouds, the shroud temperature is prescribed at the same value as the surface of the block. For nonconducting shrouds, a zero normal temperature gradient $\partial T/\partial y$ is prescribed on the shrouds.

The conservation equations describing the flow and heat transfer in this problem were solved numerically using the control-volume discretization procedure described in [9]. The computations were performed on

a Cray-1 supercomputer using a specially vectorized form of the SIMPLE algorithm. A vectorized point-by-point iteration procedure in which alternate points are visited in each pass was used to solve the discretization equations, rather than the line-by-line scheme. The vectorized version of the algorithm executed three times faster on the vector processor than did the original scalar version. The block-correction procedure described in [10, 11] was incorporated with appropriate modifications to exclude the solid portion of the domain.

The results presented here were calculated on a 33×33 grid. The grid points were distributed uniformly over most of the domain, with additional grid points added near the interface between the block and the fluid. At low Rayleigh numbers, converged solutions were obtained in a few hundred iterations of the SIMPLE procedure. At high Rayleigh numbers, the momentum and energy equations are very strongly coupled, and obtaining converged solutions often required more than a thousand iterations.

Calculations on a sequence of coarser grids demonstrated that the 33×33 grid used in this study is adequate for calculating the overall heat transfer and pressure drop to reasonable accuracy for all the problems considered here. The details of the secondary flow are accurately calculated with this grid for the cases where single-eddy solutions were obtained, but a finer grid would be required to obtain the same quantitative accuracy in the solutions where complicated multiple-eddy patterns occurred. The overall values of fRe and Nu are estimated to be accurate to within 2% for the cases with single-eddy solutions, and to within 5% for cases with multiple-eddy solutions.

RESULTS AND DISCUSSION

Solutions were obtained for the range of Rayleigh numbers from 0 to 10^6 for the five different physical situations summarized in Table 1, covering both the regular geometry shown in Fig. 2(a) and the inverted geometry, nonconducting shrouds and perfectly conducting shrouds, and fluids with Prandtl number of 0.7, corresponding to air, and 3.5, for liquid freon. The authors are not aware of any existing experimental data with which to compare the numerical results for the fully developed mixed convection regime in this geometry. To establish the applicability of a laminar-flow analysis to practical electronic devices, an estimate of the dimensionless parameters will now be made. Typical values of the dimension H and the heating rate Q' are 0.5 cm and 1 kW m^{-1} respectively. With air as the working fluid, flowing at 2 m s^{-1}, the corresponding Reynolds number is about 1400 and the Rayleigh number is 4×10^5. Thus the analysis presented here is applicable to many real devices.

Table 1. Different physical situations considered

Case	Geometry	Shrouds	Prandtl number
1	regular	non-conducting	0.7
2	inverted	non-conducting	0.7
3	regular	perfectly conducting	0.7
4	inverted	perfectly conducting	0.7
5	regular	non-conducting	3.5

Streamlines and isotherms

The structure of the secondary flow and its effect on the temperature field will now be shown via contour plots of the streamlines and the isotherms for a few representative cases. To establish a reference pattern for the isotherms, it is of interest to consider first the forced convection solution ($Ra = 0$). The forced convection isotherms are shown in Fig. 3, for the cases of nonconducting shrouds and perfectly conducting

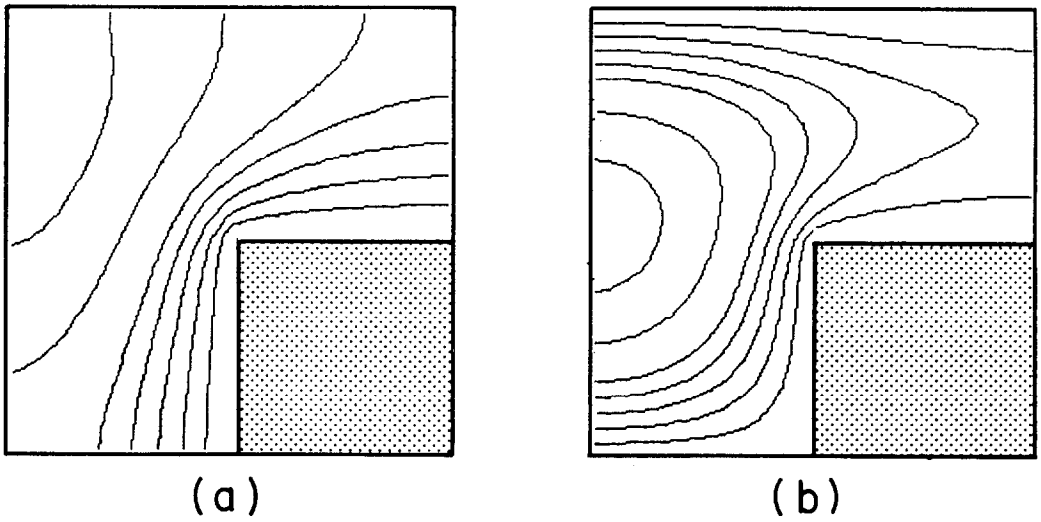

FIG. 3. Isotherms for forced convection ($Ra = 0$). (a) Non-conducting shrouds; (b) perfectly conducting shrouds.

shrouds. These patterns do not depend on the Prandtl number, nor are they affected by the orientation of the geometry. The only effect of inverting the geometry is to change the direction of the gravitational body force, which plays no role in forced convection. The conductivity of the shrouds does, however, have a strong effect on the temperature field. When the shrouds are highly conductive, they act like fin surfaces, leading to significantly more heat transfer. The difference between the isotherms in Fig. 3 and those to be shown in Figs. 4–7 represents the distortion of the temperature field caused by the buoyancy-induced secondary flow.

In the representation of the secondary flow and temperature fields in Figs. 4–7, the symmetry of the problem is utilized to display the isotherms in the left half of each figure and the streamlines in the right half. To plot the streamlines, a dimensionless stream function is defined by:

$$\frac{\partial \psi}{\partial Y} = U \tag{14}$$

$$\frac{\partial \psi}{\partial X} = -V. \tag{15}$$

The maximum value ψ_m of the stream function is a measure of the strength of the secondary flow, and is listed for each figure.

The streamlines and isotherms for Case 1 are shown in Fig. 4 for $Ra = 10^6$. The solutions of the governing equations are found to be non-unique at high Rayleigh numbers for this configuration. Both single-eddy and double-eddy solutions were obtained for Rayleigh numbers in excess of 10^4 in this case. The single-eddy solutions feature one clockwise rotating vortex. The isotherm pattern shows steeper temperature gradients and consequently thinner thermal boundary layers on

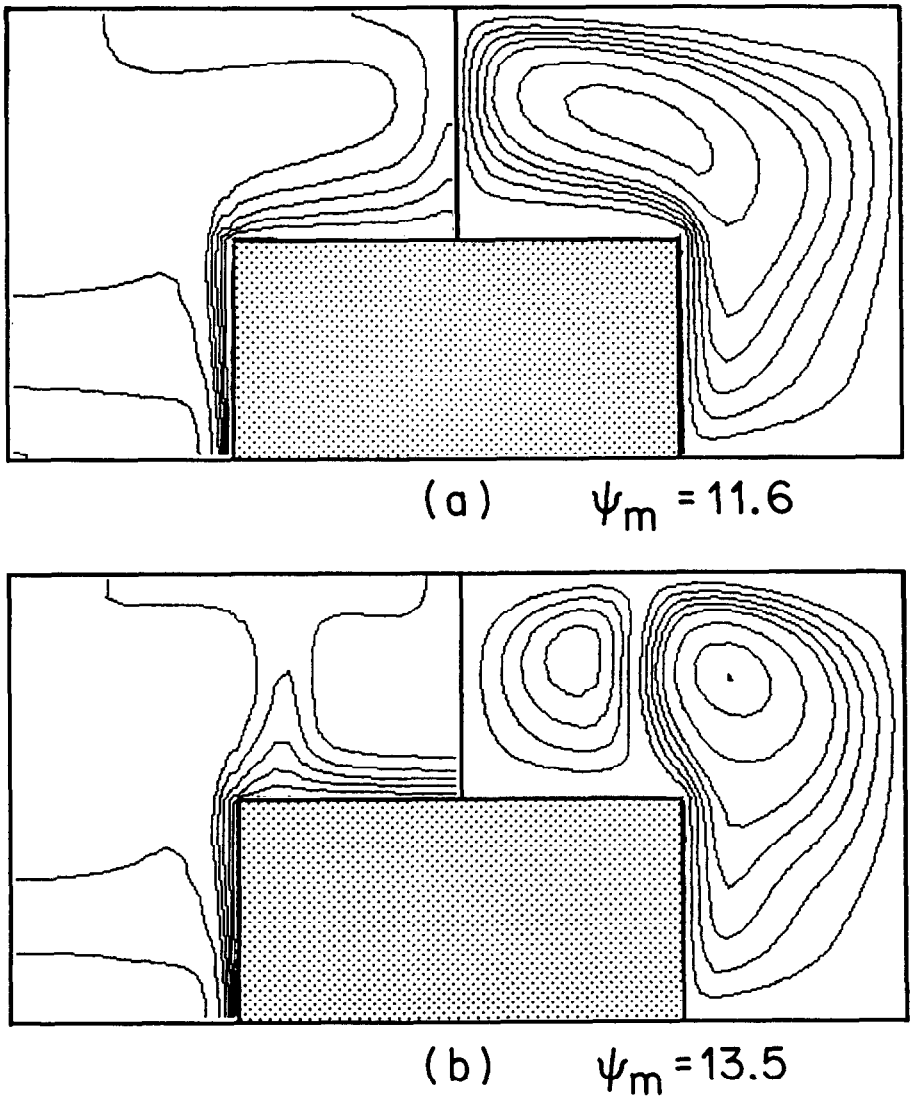

FIG. 4. Isotherms and streamlines for Case 1, $Ra = 10^6$. (a) Single-eddy solution; (b) Double-eddy solution.

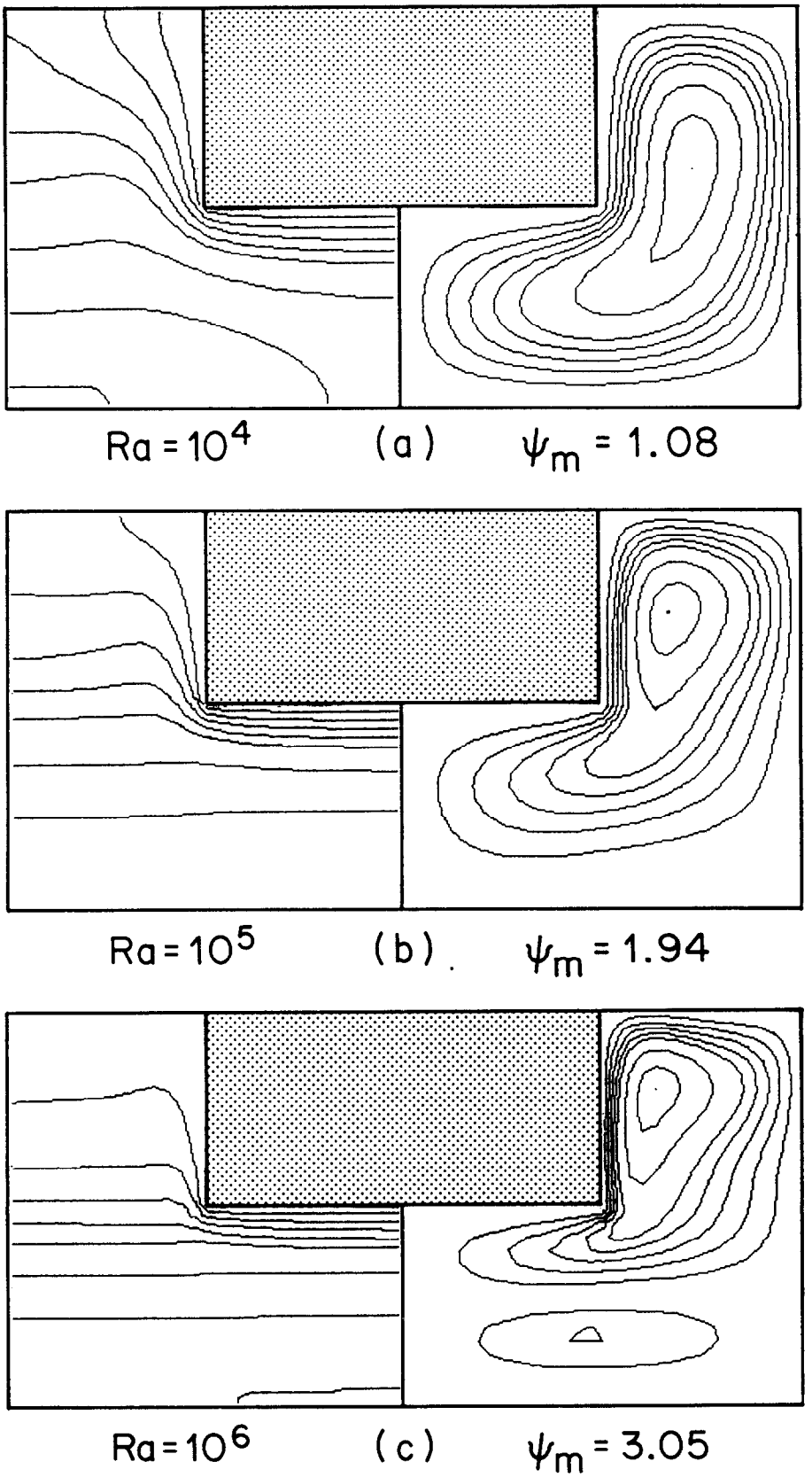

FIG. 5. Isotherms and streamlines for Case 2.

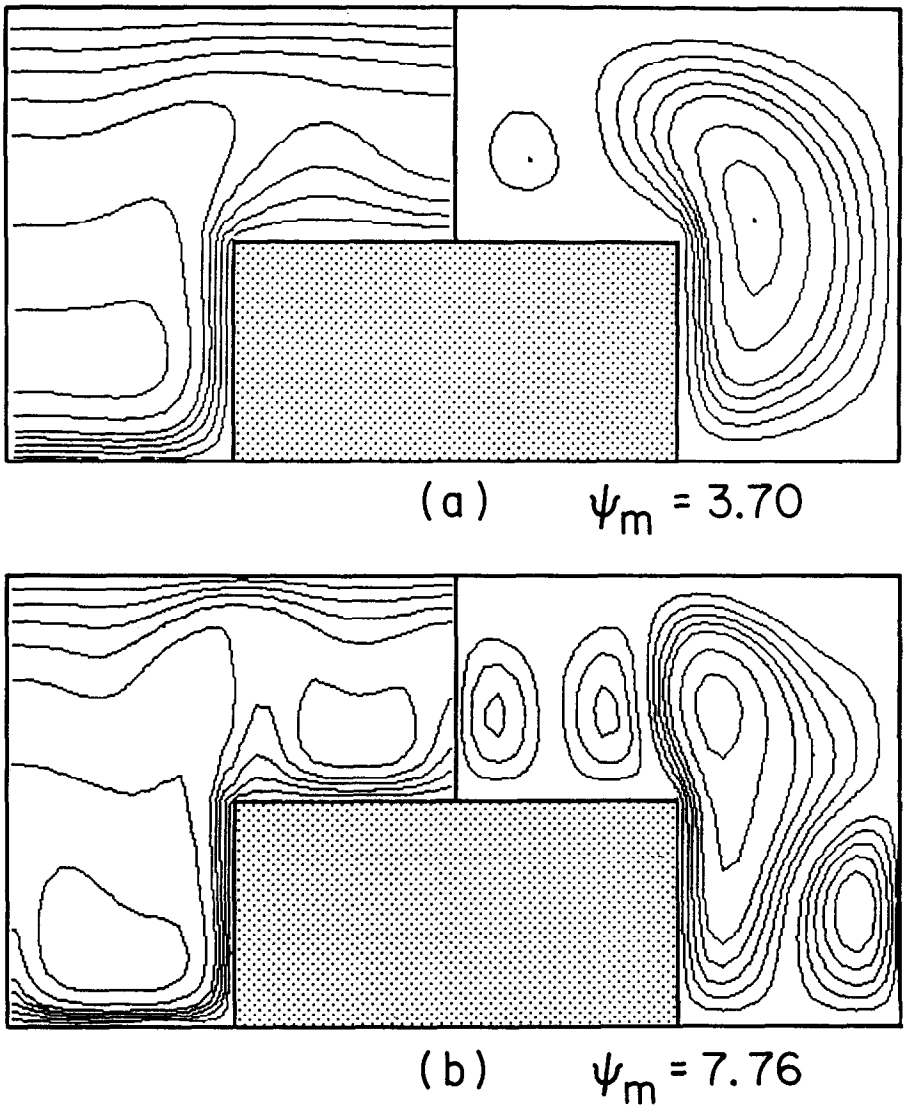

FIG. 6. Isotherms and streamlines for Case 3. (a) $Ra = 10^5$; (b) $Ra = 10^6$.

both the vertical and top faces of the block than were seen for the forced convection case, demonstrating the enhancement of heat transfer due to buoyancy. The double-eddy solution is characterized by the presence of a weak second eddy directly above the block rotating in the opposite direction to the main eddy. The presence of this eddy causes the thermal boundary layer on the top face of the heated block to be somewhat thinner than for the single-eddy solution.

Although extensive consideration of the phenomena of multiple solutions in this problem is beyond the scope of this paper, some comments are in order. Single-eddy patterns for the secondary flow were always obtained for Rayleigh numbers below 10^3. The resulting secondary flow was somewhat stronger for the double-eddy solutions than for the corresponding single-eddy solutions. Comparison of the patterns in Fig. 4 for the single and double-eddy solutions shows that the main difference is in the region above the block; the streamlines and isotherms in the main part of the flow are very similar. Since the main part of the flow is insensitive to the details of the flow in the region above the block, it is expected that the overall heat transfer and pressure drop will not be greatly affected. Thus, the fact that multiple solutions exist is not of great practical significance.

The results for the inverted geometry (Case 2) are shown in Fig. 5. The secondary flow pattern consists of a large clockwise-rotating eddy at $Ra = 10^4$ and 10^5. At $Ra = 10^6$, a small counter-clockwise rotating eddy appears directly below the main eddy. The secondary flow is found to be much weaker than in Case 1, where the heated blocks were facing upward. This result is not surprising, since it is well known that buoyancy effects are stronger when a fluid is heated from below than from above. The isotherm plots show a definite trend

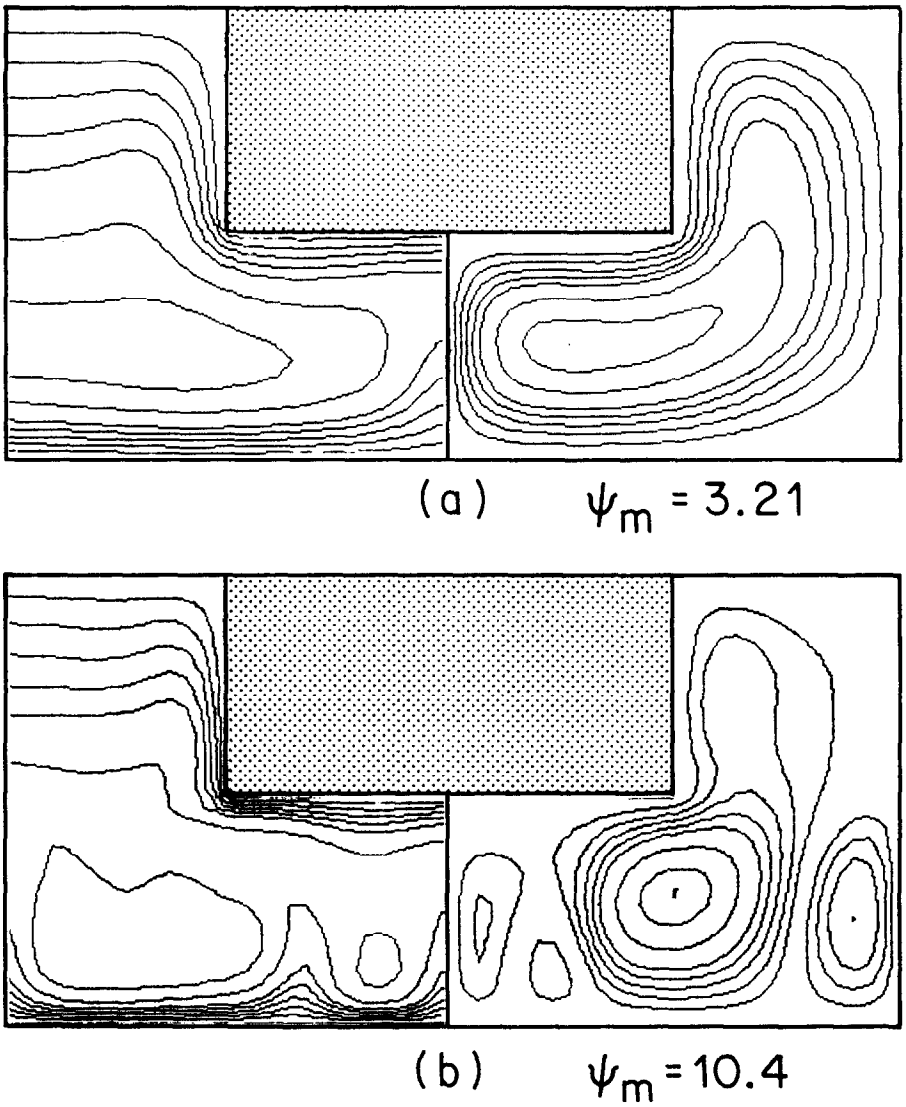

FIG. 7. Isotherms and streamlines for Case 4. (a) $Ra = 10^5$; (b) $Ra = 10^6$.

toward increasing thermal stratification as the Rayleigh number is increased. The local heat transfer on the bottom surface of the block is enhanced, but the heat transfer from the vertical face of the block appears to be poor. Consequently, the enhancement of heat transfer resulting from buoyancy in the inverted geometry is less than that in the original geometry.

Figure 6 pertains to Case 3, where the highly conductive shrouds act as heated surfaces. The isotherm plots show that the thermal boundary layers along the surfaces of the block and the shrouds get thinner as the Rayleigh number is increased, indicating improved heat transfer. Compared with Case 1, the secondary flow here is significantly weaker. This is to be expected, since the heating of the top surface reduces the temperature nonuniformity in the fluid. The complicated flow pattern for $Ra = 10^6$ is not claimed to be a quantitatively accurate solution, since all the fine details of the flow cannot be properly resolved on the 33×33 grid used in this study. The two major eddies, however, are accurately predicted, and the weak secondary motion associated with the two other eddies has rather small effect on the overall heat transfer and pressure drop. A closer examination of this flow field reveals some interesting features. The region directly above the heated block contains two eddies of equal size rotating in opposite directions, which is the flow pattern that occurs in a square channel that has heated surfaces on the top and bottom and insulated sides. The streamline pattern to the right of the block, with a large eddy and a smaller counter-rotating eddy in the bottom corner, is very similar to that reported in [6] for mixed convection between hot fins. It appears as though the flow in the region above the block and the flow to the right of the block behave independently of one another under these conditions.

The isotherms and streamlines for Case 4 are presented in Fig. 7. The streamlines for $Ra = 10^5$ are

somewhat similar to those of Case 2, except that the center of the eddy is shifted downward to a position below the block. The secondary flow pattern for $Ra = 10^6$ is again rather complicated and the comments made for the accuracy of the solution for Fig. 6(b) apply here as well. The effect of the inversion of the geometry on the strength of the secondary flow is less clear-cut for Cases 3 and 4 than for Cases 1 and 2. This is because the heated shrouds in Cases 3 and 4 provide heating to the fluid from both above and below, in either orientation of the geometry.

The results for Case 5, which are not shown here, are very similar to those of Case 1. The two cases differ only in the value of the Prandtl number. Not only are the isotherms and streamlines for the two cases very similar, but the strength of the secondary flow, as measured by ψ_m, is also about the same. These observations show that the Rayleigh number indeed accounts for a large part of the Prandtl number dependence in the problem, even when the Prandtl number is as low as 0.7. The Rayleigh number is thus a better choice as the parameter to characterize the strength of the buoyancy effects in this problem than is the Grashof number.

Overall heat transfer coefficient

For design purposes, the overall heat transfer and pressure drop in the device are of primary interest. The overall heat transfer results are conveniently presented in the form of the Nusselt number $Nu = hH/k$, and the ratio Nu/Nu_0, where Nu_0 is the Nusselt number corresponding to the forced convection case.

The average heat transfer coefficient h is defined here such that:

$$h = Q'/[A_b(T_w - T_b)] \tag{16}$$

where A_b is the heated surface area of the rectangular block only. It should be noted that, when the shrouds are conducting, their area is not included in the heated area in the definition of the heat transfer coefficient. The result is that the calculated Nusselt numbers represent a measure of the amount of heat transferred for the same $(T_w - T_b)$.

Figure 8 shows a plot of the Nusselt number vs Rayleigh number for the five cases considered. It may be recalled that Cases 1–4 differed in the orientation of the heated blocks and in the thermal boundary conditions imposed on the shrouds, but that all were for $Pr = 0.7$. Case 5 was for $Pr = 3.5$, and will be considered separately. In general, the Nusselt number increases with the Rayleigh number. It can be seen that the Nusselt number is significantly influenced by the thermal boundary conditions imposed on the shrouds. The two cases with highly conducting shrouds have higher Nusselt numbers because the conducting shrouds act as extended surfaces for heat transfer. The dashed line identified as Case 1* gives the implications of the double-eddy solutions obtained for Case 1. The Nu values for the double eddy case are somewhat higher than for the single-eddy case, with the difference

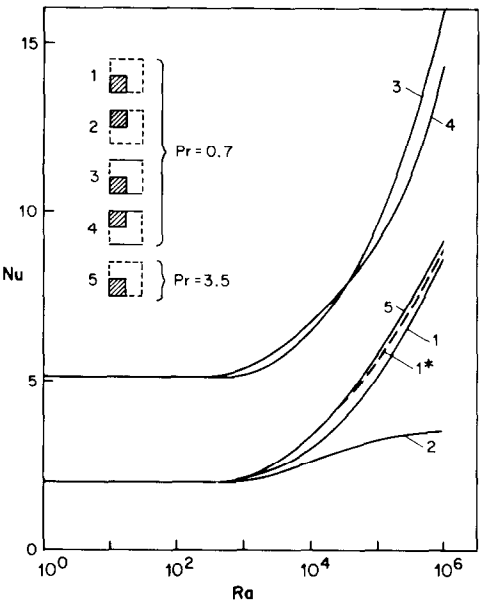

FIG. 8. Effect of buoyancy on Nusselt number.

ranging from 16% at $Ra = 10^4$ to 3% at $Ra = 10^6$.

It is interesting to note the range of Nusselt numbers involved in Fig. 8: from a low of 2.0 for forced convection in Cases 1 and 2 to a high of 15.9 for Case 3 at a Rayleigh number of 10^6. Thus, the combined effects of buoyancy and highly conductive shrouds increase the heat transfer by a factor of eight over the forced convection case with nonconducting shrouds. Clearly, buoyancy effects must be taken into consideration in design calculations.

The effect of Prandtl number on the Nusselt number is seen to be quite small, as comparison of the curves for Cases 1 and 5 reveals. The Nusselt number increases only slightly with increasing Prandtl number.

The effect of buoyancy is seen more clearly from the ratio Nu/Nu_0, which is presented in Fig. 9. The curves in the upper left-hand corner of the figure pertain to the friction-factor ratio and will be discussed later. The enhancement in the Nusselt number is noticeable only for Rayleigh numbers greater than about 10^3. For $Pr = 0.7$, the largest Nusselt number ratios are encountered in Case 1. This is not surprising since Case 1 also had the strongest secondary flows. The double-eddy solutions for Case 1 are again indicated by the dashed line marked 1*. In Case 3, the heated shroud surface at the top reduces the temperature gradients in the fluid, leading to weaker secondary flow, and a correspondingly lesser improvement in heat transfer. Cases 2 and 4, with the inverted geometry in which the heated blocks are mounted facing downward, show less enhancement of heat transfer than the corresponding cases with the original geometry. The difference between Cases 1 and 2 is seen to be greater than that between 3 and 4. All these trends are in conformity with the behavior observed for the streamline and isotherm patterns.

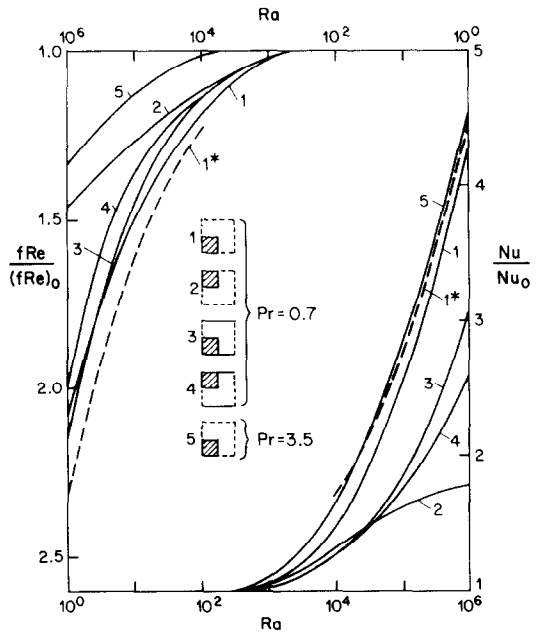

FIG. 9. Nussselt number ratio and friction factor ratio as functions of Rayleigh number.

Friction factor

The axial pressure drop for the flow can be expressed in terms of the friction factor f, where f is given by the standard definition:

$$f = \frac{(-\mathrm{d}\bar{p}/\mathrm{d}z)D_h}{1/2\rho\bar{w}^2}. \tag{17}$$

The hydraulic diameter D_h for this problem is given by:

$$D_h = \frac{4(\text{cross-sectional area})}{(\text{wetted perimeter})} = 2\left(\frac{c(l+s)-Hl}{l+s+H}\right). \tag{18}$$

In terms of the dimensionless variables, the result can be written as:

$$fRe = \frac{8}{\bar{W}}\left(\frac{C(L+S)-L}{L+S+1}\right)^2 \tag{19}$$

where the Reynolds number $Re = \bar{w}D_h/\nu$.

In the absence of the secondary flow, the fully developed value of fRe for the geometry considered here is 77.4; this will be denoted by $(fRe)_0$, with the subscript indicating a zero Rayleigh number. The variation of $fRe/(fRe)_0$ with Rayleigh number for the five cases considered is also shown in Fig. 9; the top and left-hand scales are to be used for these curves. In general, the behavior of the friction factor ratio is similar to that of the Nusselt number ratio, although the relative enhancement of heat transfer is significantly greater than the corresponding increase in pressure drop. For example, Case 1 at $Ra = 10^6$ shows a fourfold improvement in heat transfer over the forced convection case, with only a twofold increase in pressure drop.

The effect of Prandtl number on the friction factor can be seen from comparison of the curves for Cases 1 and 5. The increase in friction factor due to buoyancy is seen to be significantly less for the fluid with the larger Prandtl number. It can be seen from the governing differential equations that as the Prandtl number approaches infinity, the axial momentum equation becomes uncoupled from the energy equation, and the friction factor assumes its forced convection value. Thus, the use of high Prandtl number fluids is advantageous since the enhancement of heat transfer due to buoyancy is achieved at a smaller penalty in increased pressure drop.

CONCLUDING REMARKS

The numerical investigation presented here demonstrates that buoyancy effects have a significant effect on the fully-developed laminar flow and heat transfer through shrouded arrays of rectangular blocks. The secondary flow induced by buoyancy leads to a significant enhancement in heat transfer over the forced convection results, along with a smaller increase in pressure drop. Since the geometry analyzed here is similar to that found in many modern electronic devices, the importance of the mixed convection regime in the thermal analysis of electronic equipment is apparent. Several factors were identified that lead to improved heat transfer performance. Mounting the heated blocks facing upward, the inclusion of highly conductive shrouds, and the use of high Prandtl number fluids all lead to enhanced heat transfer.

Acknowledgments—This research was performed under the auspices of National Science Foundation Grant NSF/MEA-8116961 A01. The computational costs were partially covered by a grant from the University of Minnesota Computer Center.

REFERENCES

1. U. P. Hwang and K. P. Moran, Boiling heat transfer of silicon integrated circuits chip mounted on a substrate. In *Heat Transfer in Electronic Equipment* (edited by M. D. Kelleher and M. M. Yovanovich). American Society of Mechanical Engineers, New York (1984).
2. E. M. Sparrow and A. Chukaev, Forced-convection heat transfer in a duct having spanwise-periodic rectangular protuberances, *Num. Heat Transfer* **3**, 149–167 (1980).
3. W. N. Gill and E. Del Casale, A theoretical investigation of natural convection effects in forced horizontal flows, *A.I.Ch.E. Jl* **8**, 513 (1962).
4. K. C. Cheng and G. J. Hwang, Numerical solution for combined free and forced laminar convection in horizontal rectangular channels, *J. Heat Transfer* **91**, 59–66 (1969).
5. K. J. Kennedy and A. Zebib, Combined free and forced convection between horizontal parallel planes: some case studies, *Int. J. Heat Mass Transfer* **26**, 471–474 (1983).
6. S. Acharya and S. V. Patankar, Laminar mixed convection in a shrouded fin array, *J. Heat Transfer* **103**, 559–565 (1981).
7. A. Nieckele and S. V. Patankar, Mixed convection in a concentric annulus with horizontal axis, ASME paper 83-HT-74 (1983).

8. S. V. Patankar, A numerical method for conduction in composite materials, flow in irregular geometries and conjugate heat transfer. *Proc. 6th International Heat Transfer Conference*, Toronto, Vol. 3, p. 297 (1978).
9. S. V. Patankar, *Numerical Heat Transfer and Fluid Flow*. McGraw-Hill, New York (1980).
10. A. Settari and K. Aziz, A generalization of the additive corrrection methods for the iterative solution of matrix equations, *SIAM J. Num. Analysis* **10**, 506 (1973).
11. S. V. Patankar, A calculation procedure for two-dimensional elliptic situations, *Num. Heat Transfer* **4**, 409–425 (1981).

ANALYSE DE LA CONVECTION MIXTE LAMINAIRE DANS DES ARRANGEMENTS DE BLOCS RECTANGULAIRES CHAUFFES

Résumé—On étudie numériquement l'effet de la pesanteur sur l'écoulement et le transfert thermique dans des arrangements de blocs rectangulaires. Le problème considéré est relatif au refroidissement d'un équipement électronique fait de composants montés sur des circuits imprimés horizontaux. Les effets de l'orientation des blocs, la conduction dans les épaulements et les proprietétés des fluides sont considérés. On calcule les champs de vitesse et de température. Les résultats montrent que la pesanteur conduit à un accroissement significatif du transfert thermique et une faible augmentation de la perte de charge s'associe au plus grand accroissement quand les blocs chauffés font face vers le haut. L'écoulement secondaire forme un tourbillon unique aux faibles nombres de Reynolds et des configurations à un seul ou plusieurs tourbillons aux nombres de Rayleigh élevés.

UNTERSUCHUNGEN DER LAMINAREN MISCHKONVEKTION IN UMHÜLLTEN ANORDNUNGEN VON BEHEIZTEN RECHTECKIGEN BLÖCKEN

Zusammenfassung—Der Einfluß des Auftriebs auf die Strömung und Wärmeübertragung in umhüllten Anordnungen von rechteckigen Blöcken wird numerisch untersucht. Das betrachtete Problem tritt bei der Kühlung von elektronischen Geräten auf, deren Komponenten auf horizontalen Platten angebracht sind. Es wurden der Einfluß der Ausrichtung der Blöcke, die Wärmeleitung innerhalb der Umhüllung und die Eigenschaften des Fluids berücksichtigt und detaillierte Geschwindigkeits- und Temperaturfelder berechnet. Die Ergebnisse zeigen, daß der Auftrieb zu einer wesentlichen Steigerung der Wärmeübertragung bei einem geringerem Anstieg des Druckabfalls führt. Die größte Verbesserung tritt dann auf, wenn die beheizten Blöcke von der Platte nach oben ragen. Die Sekundärströmung bildet für kleine Rayleigh-Zahlen Einzelwirbel, wohingegen für größere Rayleigh-Zahlen Einzel- und Mehrfach-Wirbel entstehen.

АНАЛИЗ ЛАМИНАРНОЙ СМЕШАННОЙ КОНВЕКЦИИ В СКРЕПЛЕННЫХ РЕШЕТКАХ ИЗ НАГРЕТЫХ ПРЯМОУГОЛЬНЫХ БЛОКОВ

Аннотация—Численно исследуются влияние подъемных сил на течение и теплообмен в скрепленных решетках из прямоугольных блоков. Рассматриваемая задача относится к охлаждению электронного оборудования, составленного из элементов, смонтированных на горизонтальных платах. Рассматривается влияние ориентации блоков, теплопроводности перемычек и свойств жидкости. Рассчитаны поля скорости и температуры. Результаты показывают, что подъемные силы вызывают существенную интенсификацию теплообмена одновременно с небольшим ростом падения давления, причем найдено, что наибольшая интенсификация имела место в том случае, когда нагретая поверхность блоков ориентирована вверх. Вторичное течение образует одновихревые структуры при малых числах Рэлея и, как одно-, так и многовихревые структуры при больших числах Рэлея.